Quantum entanglement in polarization and space
Lee, Peter Sing Kin

CHAPTER 4

Increased polarization-entangled photon flux via thinner crystals

We analyze the scaling laws that govern the production of polarization-entangled photons via type-II spontaneous parametric down-conversion (SPDC). We demonstrate experimentally that thin nonlinear crystals can generate a higher number of entangled photons than thicker crystals, basically because they generate a broader spectrum.

4.1   Introduction

Spontaneous parametric down-conversion (SPDC) has become the standard tool to gener-
ate entangled photon pairs for experimental studies on the foundations of quantum mechan-
ics [6–8]. These photon pairs can be simultaneously entangled in energy, momentum, and
polarization (for type-II SPDC), but the use of polarization entanglement is most popular due
to its simplicity. Although the mathematical description of the generating process is well
known [20, 35], we think that its physical implications are not yet fully exploited. We hereby
refer specifically to the thickness of the nonlinear crystal, which for BBO is generally chosen
between 0.5-3 mm without any further justification [8, 23]. In this paper, we will discuss the
role of the crystal thickness in terms of simple scaling laws and show that the production rate
of entangled pairs can actually be increased considerably by *reducing* the crystal thickness
(to 0.25 mm in our case). Our treatment is restricted to the case of a cw pump, but can be
extended to pulsed pumping.

   The theoretical description of type-II SPDC is centered around the two-photon wave func-
tion $\Phi(\mathbf{q}_o, \mathbf{q}_e; \omega_o, \omega_e)$, which quantifies the probability amplitude to generated a photon pair
with transverse momentum $\mathbf{q}_i$ and frequency ω_i, for the ordinary ($i = o$) and extra-ordinary
($i = e$) polarization, respectively. Stripped down to its bare essentials this two-photon wave
function is

$$|\Phi(\mathbf{q}_o, \omega_o; \mathbf{q}_e, \omega_e)| \propto L \text{sinc}(\Delta\phi) \,, \tag{4.1}$$

where L is the crystal thickness, $\text{sinc}(x) = \sin(x)/x$, and $\Delta\phi = L\Delta k$ is the phase mismatch.
If the pump laser is an almost plane-wave beam at normal incidence, conservation of energy
and transverse momentum requires that $\omega_o + \omega_e = \omega_p$ and $\mathbf{q}_o + \mathbf{q}_e = \mathbf{0}$, and $\Delta\phi$ becomes
a function of one frequency and transverse momentum only. This functional dependence
is such that the two polarized components are emitted in angular cones that are displaced
with respect to the pump over an angle $\pm\theta_{\text{off}}$ and that are approximate mirror images of
each other (at $\omega_o \approx \omega_e$). We consider SPDC emission close to frequency degeneracy, where
$\omega_e \equiv \omega_p/2 + \delta\omega_e$ with $\delta\omega_e \ll \omega_p/2$ and ω_p as pump frequency, and linearize the phase
mismatch around an orthogonal crossing of the two SPDC cones (set by the crystal angle)
to [35, 48]

$$\Delta\phi = L\Delta k \approx \left(\frac{\partial \Delta k}{\partial \omega_e} \delta\omega_e + \frac{\partial \Delta k}{\partial \theta_{\mathbf{x}}} \delta\theta_{\mathbf{x}} + \frac{\partial \Delta k}{\partial \theta_{\mathbf{y}}} \delta\theta_{\mathbf{y}} \right) L \approx 2\pi \left(-\frac{\delta\lambda_e}{\Delta\lambda_{\text{SPCD}}} + \frac{\delta\theta_r}{\Delta\theta_{\text{SPDC}}} \right) \,, \quad (4.2)$$

where $\delta\theta_r$ measures the angle change in the radial direction. As the partial derivatives
of Δk are determined by material constants, both the spectral width $\Delta\lambda_{\text{SPDC}}$ (at fixed angle)
and the angular width $\Delta\theta_{\text{SPDC}}$ (at fixed frequency) are inversely proportional to the crystal
thickness L. More specifically, the product $\Delta\lambda_{\text{SPDC}} \times L \approx \lambda^2/[n_{gr,o} - n_{gr,e}(\theta)]$ (with $\lambda = 2\lambda_p$)
depends on the difference between two group refractive indices [53], whereas the product
$\Delta\theta_{\text{SPDC}} \times L = \lambda/\sqrt{2}\rho$ depends on the internal walk-off angle ρ.

   Typical numbers for type-II SPDC in BBO, where down-conversion from 407 to 814 nm
requires a cut-angle of about 41.2°, are as follows. Conversion of the literature values for
the refractive indices to group indices gives $\Delta\lambda_{\text{SPDC}} \times L \approx 11.5$ nm.mm. With an internal

walk-off angle $\rho = 72$ mrad (corresponding to an offset angle $\theta_{\text{off}} = 57$ mrad), the product $\Delta\theta_{\text{SPDC}} \times L \approx 8.0$ mrad.mm. Note that $\Delta\lambda_{\text{SPDC}}$ and $\Delta\theta_{\text{SPDC}}$ are specified in terms of the width of the SPDC signal from its peak value to the first minimum of its sinc^2-shaped intensity profile, making the full widths at half maximum (FWHMs) 0.89 times as large.

The simple equations (4.1) and (4.2) already present the essential scaling behavior of SPDC. For a fixed and sufficiently small detection bandwidth and opening angle, Eq. (4.1) shows that the number of detected photon pairs ($\propto |\Phi|^2$) scales as L^2 and thereby increases rapidly with crystal thickness. However, as the angular width of the SPDC rings is proportional to $1/L$, the useful crossing areas scale as $1/L^2$ and the number of photon pairs within these areas (and within a fixed spectral bandwidth) is independent of the crystal thickness. Furthermore, as the SPDC bandwidth is also proportional to $1/L$ the spectrally-integrated power is expected to scale as $1/L$, being considerably larger for a thin crystal than for a thicker one.

The scaling behavior described above should work not only for free-space detection behind apertures but also for fiber-coupled detectors, under the condition that three relevant transverse sizes are matched [23]. Specifically, optimum collection efficiency is obtained when the size of the backward propagated fiber mode is matched to the size of the pump spot. Both these sizes should be roughly equal to the transverse beam walk-off $L\rho$ to create the best overlap between the SPDC emission and the fiber mode. Under these matching conditions the spectrally-integrated photon yield for a fiber-coupled system should also scale as $1/L$ [54]. In this chapter, we will present experimental data for free-space detection only.

For pulsed instead of cw pumping the described scaling behavior remains basically the same. Although the phase mismatch in Eq. (4.2) will acquire an extra term of the form $L(\partial\Delta k/\partial\omega_p)\delta\omega_p$, the scaling of the SPDC angular and spectral width remains unchanged, making the number of useful entangled pairs again proportional to $1/L$. For more sophisticated experiments that require two simultaneously entangled photon pairs there is a catch: as the two pairs should be temporally coherent the increased spectral bandwidth $\Delta\omega_{\text{SPDC}}$ can only be capitalized on if it remains below than the inverse pulse duration. At fixed detection bandwidth and with the proper angular scaling the SPDC yield and the production rate of double pairs will in fact be independent of the crystal thickness.

4.2 Measurements and results

The experimental setup is shown in Figure 4.1. Light from a cw krypton ion laser operating at 407 nm is mildly focused (spot size ≈ 0.3 mm) onto a 0.25-mm-thick type-II BBO crystal (cutting angle $40.9°$) which is slightly tilted to generate "orthogonal crossings" (separated by $2\theta_{\text{off}}$). A half-wave plate and two compensating crystals (of 0.13-0.14 mm thickness) compensate for the longitudinal and transverse walk-off of the SPDC light. In the two intersection lines of the emission cones, collimating lenses of $f = 20$ cm are placed at 20 cm from the generating crystal, directly followed by apertures (diameter up to 5 mm) acting as spatial selectors. This compact setup facilitates the collection of photons in a large space angle. The light emerging from the apertures is focused by $f = 2.5$ cm lenses onto free-space single photon counters (Perkin Elmer SPCM-AQR-14). Polarizers and interference and/or red filters are used for polarization and spectral bandwidth selection, respectively. Finally, an electronic

circuit receives the output signals of the photon counters and records the coincidence counts within a time window of 1.76 ns.
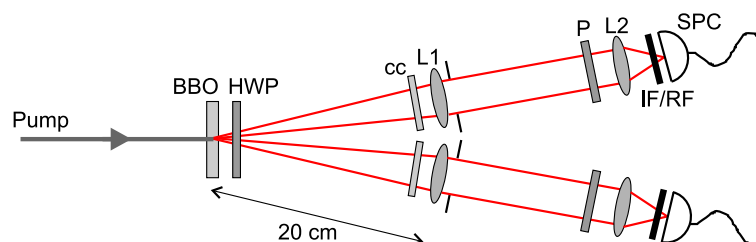

Figure 4.1: *Schematic view of the experimental setup. A cw krypton ion laser operating at 407 nm pumps a 0.25-mm-thick BBO crystal. The generated photon pairs are collected with f = 20 cm collimating lenses (L1), spatially selected by apertures and focused with f = 2.5 cm lenses (L2) onto single photon counters (SPC). Walk-off effects are compensated for by a half-wave plate (HWP) and two compensating crystals (cc) of 0.13-0.14 mm thickness. Polarizers (P) and interference/red filters (IF/RF) are used for polarization and bandwidth selection, respectively.*

Figure 4.2 depicts our key message in the form of two SPDC emission patterns for BBO crystals with thicknesses of $\approx$1 mm (measured 0.94 mm) and 0.25 mm. These pictures were measured with an intensified CCD (Princeton Instruments PI-MAX 512HQ) positioned at 6 cm from the BBO crystal behind an interference filter (5 nm spectral width) and two blue-coated mirrors that block the pump beam; no imaging lens was used. The left picture shows that the SPDC rings emitted by the 1-mm-thick BBO are relatively narrow, having a radial width of $\Delta\theta_{SPDC}$ = 10.5$\pm$1.3 mrad (FWHM). However, this value is somewhat larger than the true width of the rings since broadening by the $\approx$ 0.3-mm-wide pump spot is still considerable at 6 cm from the BBO. We measured the true radial width of $\Delta\theta_{SPDC}$ = 8.7$\pm$0.7 mrad for an increased BBO-CCD distance of both 12 and 24 cm. The right picture shows that the 0.25-mm-thick BBO emits much wider rings, with a measured radial width of $\Delta\theta_{SPDC}$ = 30$\pm$2 mrad (FWHM) (also for 12 cm BBO-CCD distance). Note that the area within the small black circles drawn in this picture is the part of the crossings selected by 5 mm diameter apertures (25 mrad), being about $(25/30)^2 \approx$ 70% of the total crossing area. The measured radial widths for both crystals are in good agreement with the expected values and scale well with the crystal thickness. For comparison, we note that the angular distance between the pump and the center of the orthogonal ring crossings is measured to be 57$\pm$1 mrad for both crystals, which indeed agrees very well with the theoretical value of θ_{off} (i.e., 57 mrad).

Figure 4.3 shows the spectral distribution of the SPDC light, measured for *H*- and *V*-polarization in one of the beams (5 mm apertures). After subtraction of the dark counts $(180~s^{-1})$ and correction for the spectral efficiency of both grating spectrometer and photon counter [55], we obtained full widths at half maxima of 51 and 44 nm for the *H*- and *V*-polarized spectrum, respectively. These numbers are in agreement with the expected value of 46 nm, and also the observation that the *H*-polarized (*o*) spectrum is somewhat wider than the *V*- polarized (*e*) spectrum is as expected [53]. These observed spectral widths scale roughly with those reported in [23], as they are indeed about a factor of 8 larger than the numbers of 4.60 nm and 4.06 nm, which are measured for the two unpolarized SPDC beams emitted by
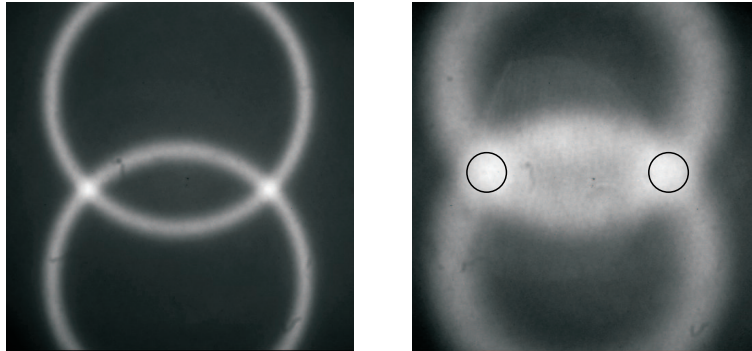
Figure 4.2: *SPDC emission patterns observed with an intensified CCD at 6 cm from (left) a 1-mm-thick BBO crystal and (right) a 0.25-mm-thick one (no imaging lens is used). The black circles on the right picture surround the SPDC crossing area selected by 5 mm diameter apertures. Both pictures cover a space angle of 220×220 mrad.*
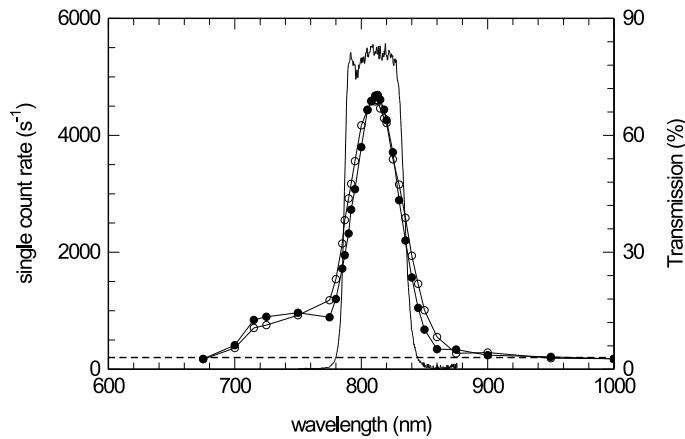

Figure 4.3: *Measured spectral distribution of the down-conversion light for H-(circles) and V-polarization (dots). The dark count level of 180 s^{-1} is indicated by the dashed line. After correction for the efficiency of both spectrometer and photon counter, we determined the central peak wavelength to be 815 nm and the peak widths (FWHM) of the H- and V-polarized light to be 51 and 44 nm, respectively. The resolution of the spectrometer is 2 nm. The solid curve (righthand scale) depicts the spectral transmission of a 50 nm broad interference filter that we used.*

a 2-mm-thick crystal in [23]. The rather prominent bump between 700 and 780 nm, which is cut off on the low-wavelength side by a red filter (Schott Glass RG715), is probably the first side maximum of the sinc^2-function, which is enhanced by the increased spectrometer throughput and detector sensitivity at lower wavelengths [55].

When using detection with free-space (bucket) detectors, there is always a trade-off between photon yield and entanglement quality. The finite size of the detection apertures as

Table 4.1: *Measured single count rates (sc), coincidence count rates (cc) and biphoton fringe visibilities $V_{45°}$ for two aperture diameters and three spectral filters: red filter RF, 50 nm and 10 nm interference filters.*

1.4 mm aperture diameter

filter	sc (10^3 s^{-1})	cc (10^3 s^{-1})	$V_{45°}$ (%)
RF	67.0	9.7	98.4
50 nm	44.9	7.8	99.0
10 nm	13.5	2.0	99.5

5 mm aperture diameter

filter	sc (10^3 s^{-1})	cc (10^3 s^{-1})	$V_{45°}$ (%)
RF	847	198	91.1
50 nm	560	145	96.0
10 nm	145	29.6	98.0

compared to the size of the crossing regions can lead to entanglement degradation by spatial labeling, whereas the finite detection bandwidth in relation to the emission bandwidth can lead to degradation by spectral labeling. The choice of our apertures (maximal diameter 5 mm) is motivated by this trade-off. In the absence of compensating crystals the combination of small apertures (diameter 1.4 mm) and narrow filters (spectral width 5 nm) still produced high-quality polarization entanglement: the biphoton fringe visibility [8] observed with the fixed polarizer oriented at 45° was $V_{45°} = 96\%$. However, a change to either a larger aperture (5 mm) or a wider filter (50 nm) seriously reduced the entanglement quality, yielding $V_{45°} = 75\%$ and $V_{45°} = 41\%$, respectively, while the combination (5 mm & 50 nm) gave $V_{45°} = 32\%$. These numbers clearly show that compensating crystals are also needed if one combines a thin generating crystal with wide apertures or a large detection bandwidth. The so-called "thin-crystal limit" is a relative concept; it only applies when the crystal is thin enough *in relation to a given detection scheme*.

In Table 4.1 we present the count rates and biphoton fringe visibilities $V_{45°}$, when using compensating crystals, measured for two aperture sizes and three different filter bandwidths at a pump intensity of 187 mW. The table quantifies the trade-off between photon yield and entanglement quality; higher count rates combine with lower entanglement quality. For all 2×3 presented cases the biphoton fringe visibility was measured to be $> 99\%$ for the *H* and *V* projection (not in Table), but is generally less for the more critical 45° projection. Although we observe a steady decrease with increasing angular detection width and/or spectral bandwidth, $V_{45°}$ is at least 96% except for one case. Based on these numbers, we consider the system with 5 mm apertures (25 mrad angular width) and 50 nm filters the most promising. Under these conditions we have measured single and coincidence rates of 560×10^3 s^{-1} and 145×10^3 s^{-1}, respectively.

To demonstrate the high brightness of our thin crystal source, we compare above rates with those obtained by us with a 1-mm-thick down-conversion crystal using 10 nm interference filters and 4 mm diameter apertures placed at 80 cm from the crystal (5 mrad space angle). For this setting, we measured singles and coincidence rates of 125×10^3 s^{-1} and 33×10^3 s^{-1}, respectively, at $V_{45^\circ} = 97.7\%$. As expected from the scaling laws, the 0.25-mm-thick crystal yields roughly about a factor 4 more photons than a 1-mm-thick one.

To put the yield of our thin SPDC source (with 5 mm apertures and 50 nm filters) in a broader perspective, we compare it with other SPDC sources reported in the literature. The first "high-intensity" source [8] used a 3-mm-thick BBO crystal and detection behind elliptical apertures (H×V sizes of 3×10 mm at 1.5 m from the crystal). This source produced a coincidence rate of 10 s^{-1}mW^{-1} (1500 s^{-1} at 150 mW pump power), which is almost 80× lower than our obtained coincidence rate of 775 s^{-1}mW^{-1}. Even an "ultrabright" source [22], based on type-I SPDC and two stacked BBO crystals of 0.59 mm thickness each, which is claimed to be 10× brighter than the one reported in [8], is still about 8× weaker than our source.

Instead of detecting entangled photons behind apertures, the use of *fiber-coupled* detectors has been introduced to several experimental schemes [23, 56, 57]. The first "high-efficiency" source based on collection with fiber-coupled detectors used a 2 mm BBO crystal to achieve a coincidence rate of as much as 900 s^{-1}mW^{-1} in the low-pump-power regime and *without polarizers*. The correct comparison is, however, with the system using polarizers for which Fig. 5 in Ref. [23] gives a coincidence rate of 225 s^{-1}mW^{-1} (obtained by division of the 90×10^3 s^{-1} fringe maximum by the 400 mW pump power). Another source [56] used a relatively thin crystal (0.5 mm BBO) to produce entangled photons at 200 s^{-1}mW^{-1}, while a compact source (2 mm BBO) [57] achieved a similar rate of 220 s^{-1}mW^{-1}.

To make a fair comparison between our free-space source and these fiber-coupled sources, we have to take into account the fact that fiber-coupled detection enables capturing of a larger area of the ring crossings. Based on our selected space angle and the actual width of the crossings (see Fig. 4.2), we expect a potential increase of our coincidence rate by about a factor 1.5, when switching to fiber-coupled detection. In practice, however, the profit will be only marginal due to the limited in-coupling efficiency in the fibers and the integration over Gaussian mode profiles instead of the sharp-edge profiles of the apertures.

4.3 Concluding discussion

In conclusion, we have discussed the scaling behavior of SPDC emission as a function of the thickness L of the generating crystal. We have found that the photon yield scales as $1/L$ if the detection angle and bandwidth are matched to the SPDC emission. A quantitative comparison of our source, with a measured coincidence rate of 775 s^{-1}mW^{-1} at $V_{45^\circ} = 96\%$, with existing sources reported in the literature (aperture and fiber-coupled), demonstrates that the use of thinner down-conversion crystals indeed yields considerably higher photon rates than thicker crystals.

How far can we go with the proposed scaling? If the yield continues to scale like $1/L$ an infinitely thin crystal would give an infinitely strong signal. The ultimate limitation is that the angular widths of the SPDC rings should be smaller than their radii to allow a discussion in

terms of SPDC rings and crossings. Before this limit is reached, there is a practical point of concern: the compensating optics and collimation lenses have to cover the full angular width of the rings, and all this has to be realized within a very limited opening angle (of 2×57 mrad). This implies an ultra-compact setup, which is even more complicated by the fact that also the beam dump for the pump laser (not shown in Fig. 4.1) has to be accommodated. In this respect, the studied BBO thickness of 0.25 mm might well be close to the optimum.

4.4   Acknowledgements